Aust. J. Phys., 1979, **32**, 105–11

On the Structure of the Crab Nebula

L. I. Matveyenko and V. I. Kostenko

Institute for Space Research, Moscow, U.S.S.R.

Abstract

Utilizing a large number of published observations, we investigate the detailed structure of the Crab Nebula over a range of wavelengths from 3·5 mm to 75 cm, and identify many different features. The spectra of some of these features are followed to longer wavelengths, extending to nearly 10 m. Physical conditions within the features are discussed.

Introduction

The brightness and polarization distributions of the Crab Nebula have been investigated by many authors from millimetre to metre wavelengths. A range of different observing techniques have been used: single-dish observations (Braun and Yen 1968; Mayer and Hollinger 1968; Kostenko and Matveyenko 1970; Matveyenko 1971; Montgomery *et al.* 1971; Matveyenko and Conklin 1972; Matveyenko and Meeks 1972); aperture synthesis (Branson 1965; Hogg *et al.* 1969; Duin and van der Laan 1972; Wilson 1972; Slee 1977); lunar occultation (Seeger and Westerhout 1957; Andrew *et al.* 1964; Lastochkin *et al.* 1965; Matveyenko *et al.* 1965; Matveyenko and Artjuch 1966; Davies *et al.* 1966; Matveyenko 1968, 1969; Artjuch *et al.* 1975); interplanetary scintillation (Hewish and Okoye 1964; Gower 1967; Matveyenko and Pynzar 1969; Cronyn 1970; Matveyenko and Lotova 1970; Armstrong *et al.* 1973); very long baseline interferometry (Erickson *et al.* 1972; Matveyenko *et al.* 1973; Vandenberg *et al.* 1973). The present paper draws on these data to provide an account of the detailed structure of the Crab Nebula and the spectra of its individual features.

Structure and Spectra of Features

Brightness temperature maps at 3·5 mm and 1·2 cm (Matveyenko 1971; Matveyenko and Conklin 1972; Matveyenko and Meeks 1972) reveal that the main emission emanates from an elliptical region of size $6'\cdot5\times4'\cdot5$ arc and orientation $\sim135°$. This region corresponds to the optical filament shell of the Crab Nebula.

The occultation data (see Fig. 1) and the aperture synthesis maps show that the boundary of the Crab Nebula coincides at all wavelengths from several centimetres to several metres, and also corresponds closely to that of the visible optical region, which has a roughly elliptical shape too. The emission from the peripheral parts of the nebula is relatively brighter at radio than at optical wavelengths, and the boundary is also steeper at radio wavelengths. However, an exception is found in the

SW. part of the nebula, where a region of weak emission is located outside the elliptical zone. This weak emission is present in both radio (Fig. 1) and optical (Woltjer 1957) maps.

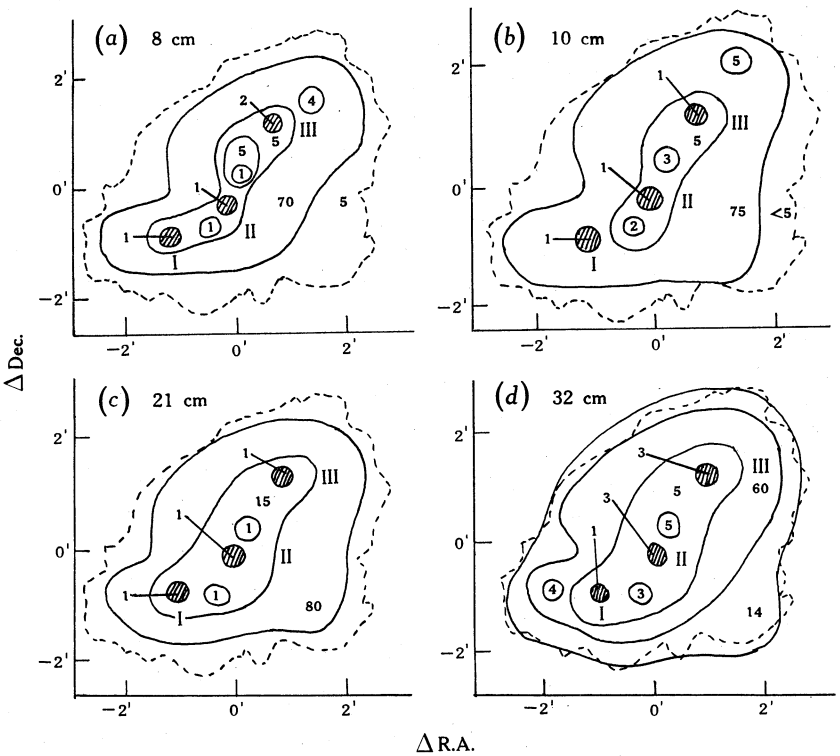

Fig. 1. Brightness distributions at the indicated wavelengths of the Crab Nebula obtained from lunar occultation data. Various regions of emission are delineated, the hatched areas representing the components I, II and III discussed in the text. The percentage of total emission associated with each region is given. The dashed curve shows the outline of the optical nebula.

The large-scale structure of the Crab Nebula can be represented by an ellipsoidal shell with its major axis lying in the sky plane. The axes of the ellipsoid are about $6'{\cdot}5 \times 4'{\cdot}5$ arc, while the thickness of the shell is $\sim 0{\cdot}2\,R$, where R is the distance of the shell from the centre of the nebula. The spectrum of this shell region is shown in Fig. 2 (crosses and accompanying curve). At decimetric wavelengths, the emission from the shell amounts to about 80% of the total flux density (small dots and dashed curve in Fig. 2) from the Crab Nebula. Spectra for three components of the nebula, for the compact source and for the pulsar are also included in Fig. 2.

Assuming the optical depth to be small, we can determine the volume emissivity of the Crab Nebula shell from the surface brightness temperatures of small areas located at angular distances from the centroid of $\sim 2'$ and $1'{\cdot}25$ arc along the directions of the major and minor axes respectively. The energy volume emissivity of the shell has a spectral index α of $-0{\cdot}38$ above 10 GHz and $-0{\cdot}14$ below 10 GHz, as can be seen from Fig. 3 (dots and accompanying curve). The change in spectral index can be interpreted within the context of a diffusion model with

synchrotron losses occurring in an assumed irregular magnetic field structure. The lifetime T of the relativistic electrons is then given by

$$T = 1{\cdot}87 \times 10^4 B^{-3/2} f_0^{-1/2} \quad \text{yr},$$

where B is the magnetic field strength in gauss and f_0 is the frequency at which the break in the slope of the shell spectrum occurs (measured in hertz). If we take

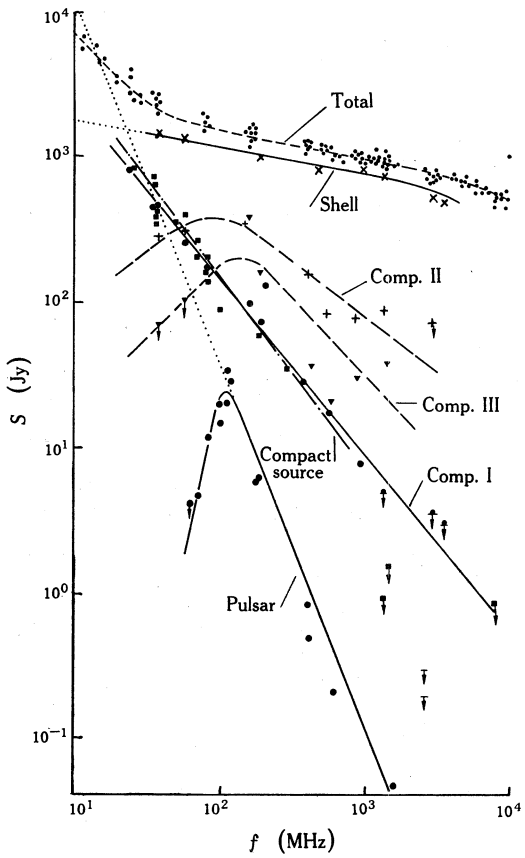

Fig. 2. Plot of flux density S versus frequency f for the Crab Nebula and its associated emission components (as indicated). The individual spectra are discussed in the text.

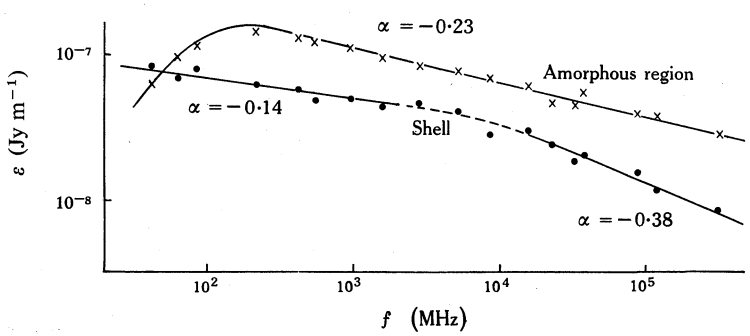

Fig. 3. Spectral variation of the volume emissivity ε of the Crab Nebula shell and of the central amorphous emitting region.

$T \approx 10^3$ yr and $f_0 \approx 10$ GHz we arrive at a magnetic field strength in the condensations of about 4×10^{-3} G.

The shell of the Crab Nebula surrounds a central amorphous emitting region of overall size $\sim 4' \times 2'$ arc along the major and minor axes. At optical wavelengths, this amorphous mass is seen to be separated into two subregions by a dark lane which coincides in orientation with the minor axis and runs through the position of the pulsar. A similar double structure for the amorphous region is seen at 56 cm in the lunar occultation observations made by Lastochkin *et al.* (1965) and Matveyenko (1968), in which the Moon's limb was parallel to the dark lane.

Radiation from the amorphous region dominates the polarized emission of the Crab Nebula. The position angle of the polarized emission at millimetre wavelengths is about 135° and corresponds to a magnetic field orientation along the minor axis. The percentage polarization at millimetre and centimetre wavelengths for the central part of the amorphous mass is 15%–20%. To the NW. side of the nebula there is a region possessing orthogonal polarization, which gives a depolarization effect when observations are made with a beamwidth larger than 1′ arc. Although the position angles of polarization for both the central and NW. regions change as λ^2, they nevertheless remain orthogonal at all wavelengths (Davies *et al.* 1966; Mayer and Hollinger 1968; Matveyenko and Conklin 1972). This indicates that the variation of the position angles with wavelength results from Faraday rotation in the interstellar medium.

The measured value of the percentage polarization at millimetre and centimetre wavelengths is smaller than that theoretically predicted for a uniform field. If we take the spectral index of the amorphous region to be $\alpha = -0{\cdot}23$ then the percentage polarization P is given by

$$P = (3-3\alpha)/(5-3\alpha) \approx 65\%.$$

This difference between the observed and calculated percentage polarizations can be attributed to an irregular magnetic field in the amorphous region, the energy of which is equal to about 50% of the total energy of the magnetic field (Burn 1966)

The volume emissivity of the amorphous mass is shown in Fig. 3 (crosses and accompanying curve). The spectral index is about $-0{\cdot}23$ at wavelengths shorter than 2 m. The spectrum decreases at longer wavelengths, which is perhaps a result of a lack of low energy electrons injected by the pulsar. The volume emissivity of the amorphous mass is higher than that of the shell at wavelengths less than 5 m.

The variation with radial distance of the spectral index of the amorphous mass in the 8 mm to 3 cm band is shown in Fig. 4. Near the centre of the mass we have $-\alpha = 0{\cdot}15$–$0{\cdot}30$, while at an angular distance of 2′–2′·5 arc we have $-\alpha = 0{\cdot}5$–$0{\cdot}6$. This variation of the spectral index is perhaps connected with synchrotron losses by the relativistic electrons in the irregular magnetic field. Let us suppose that the electrons are injected into the central region of radius r_0 and then diffuse to the periphery in a magnetic field B, which changes with radius r as

$$B \propto B_0(r/r_0)^n.$$

The discrete structure of the field can be adopted as $B = k_r B_0$, where k_r is the field strengthening factor at distance r. On the basis of a numeral calculation, we have found that the observed variation of spectral index shown in Fig. 4 can be

explained assuming $B_0 = 3 \times 10^{-4}$ G, $n = 0{\cdot}7$ and $r_0 = 10''$ arc. Then the strength of the magnetic field in the condensations is $(3\text{–}4) \times 10^{-4}$ G and the linear scale of the condensations is $\sim 3 \times 10^{16}$ cm. The total magnetic field energy is $\sim 10^{49}$ erg.

Besides these large-scale features, the Crab Nebula has some bright regions which correspond to the bright optical ones. The SE. feature labelled I in Fig. 1 is located about $\sim 1'{\cdot}5$ arc from the pulsar and has a size 10–20″ arc. Its spectrum is shown in Fig. 2, where it can be seen to possess a spectral index of $-1{\cdot}2$. Occultation observations in 1974 (Artjuch *et al.* 1975) did not reveal this component at a wavelength of $6{\cdot}5$ m. The brightness temperature of component I has decreased by a factor of more than 3 in a period of 10 years.

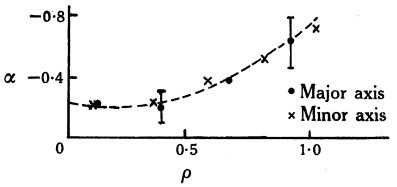

Fig. 4. Radial variation of spectral index α for the amorphous region in the 8 mm to 3 cm band. A normalized radial distance of $\rho = 1{\cdot}0$ corresponds to $3'{\cdot}25$ and $2'{\cdot}25$ arc in the major and minor axis directions respectively.

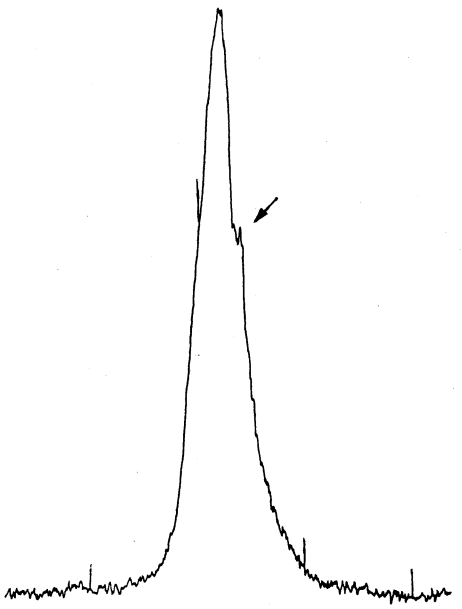

Fig. 5. Drift curve through the Crab Nebula at 8 cm on 9 June 1964, with the arrow indicating the observed variable component.

The phenomenon of variability was first observed at 8 cm on the day prior to the June 1964 occultation (Matveyenko 1975). A drift curve taken through the nebula on that day is shown in Fig. 5, the antenna beamwidth being $3'{\cdot}9 \times 11'$ arc. The feature indicated by an arrow is located $\sim 1'{\cdot}5$ arc SE. of the centre of the Crab Nebula. The flux density of this feature is $\sim 10\%$ of the total flux density of the Crab Nebula. On the following day, its flux density had fallen to less than 1% of the total. Since the lifetime of this component at 8 cm was < 1 day, its angular size and brightness temperature would be $\leqslant 0''{\cdot}1$ arc and $\geqslant 10^9$ K respectively. The emission of this component may have come from a cloud of relativistic particles moving with velocity $v \approx c$ along a magnetic tube which had a curvature radius $\sim 0{\cdot}01$ light year.

The emission beamwidth would have been about 15°. However, this interpretation presents the difficulty of explaining how a cloud of relativistic particles could maintain such a high velocity over an angular distance of $\sim 1' \cdot 5$ arc, or a linear distance of $\sim 1 \cdot 5$ light years.

In the central part of the Crab Nebula there is a region (designated II in Fig. 1), which consists of two subcomponents. Both have a size of $\sim 15''$ arc and are separated by $\sim 20''$ arc. Their combined spectrum is included in Fig. 2. In addition, in the NW. of the central part, there is a component (designated III in Fig. 1). The size of this component is 10–20″ arc; its spectrum is also included in Fig. 2.

The compact source in the Crab Nebula was measured using scintillation in the interplanetary medium (see relevant references given in the Introduction). The angular size of this source is $\geqslant 0'' \cdot 1$ arc at metre wavelengths, as determined by scattering in the irregularities of the Crab Nebula and interstellar medium (Matveyenko and Lotova 1970). The right ascension of the compact source relative to the centre of the Crab Nebula at metre wavelengths is $\Delta\alpha = -1'' \pm 6''$ arc and relative to the pulsar is $\Delta\alpha = 0'' \pm 20''$ arc (Gower 1967; Matveyenko and Pynzar 1969). The spectrum of the compact source (from the scintillation and occultation data) is also included in Fig. 2; its spectral index is $-1 \cdot 4$.

The spectrum of the compact source is different from the pulsar spectrum (Fig. 2). The flux density of the compact source is greater than that of the pulsar at wavelengths shorter than 7 m. It is possible that the excess emission from the compact source is due to radiation from other sources, such as compact wisps and/or the pulsar envelope. The variations in the pulsar pulse shape due to scattering possessing time scales of about one week or shorter also indicate that the size of the relativistic particle clouds is small (Armstrong *et al.* 1973). The spectral index of the scintillation source is close to that of component I. This coincidence is possibly due to the fact that there is a common source of injection of relativistic particles.

The spectra of the scintillating source, the component I and the pulsar indicate that the spectral index of the Crab Nebula should be steeper at decametric wavelengths. This is confirmed by decametre band observations which yield a value of about $-0 \cdot 8$ (Bazeljan *et al.* 1963).

References

Andrew, B. M., Branson, N. J. B. A., and Wills, D. (1964). *Nature* **203**, 171.
Armstrong, J. W., Coles, W. A., Kaufman, J. J., and Rickett, B. J. (1973). *Astrophys. J.* **186**, L141.
Artjuch, V. S., *et al.* (1975). *Sov. Astron. Lett.* **6**, 23.
Bazeljan, L. L., *et al.* (1963). *Izv. Vyssh. Uchebn. Zaved. Radiophys.* **6**, 897.
Branson, N. J. B. A. (1965). *Observatory* **949**, 250.
Braun, L. D., and Yen, T. L. (1968). *Astrophys. J.* **153**, L123.
Burn, B. J. (1966). *Mon. Not. R. Astron. Soc.* **133**, 67.
Cronyn, W. M. (1970). *Proc. Astron. Soc. Pac.* **82**, 1028.
Davies, R. D., Gardner, F. F., Hazard, G., and Mackey, M. B. (1966). *Aust. J. Phys.* **19**, 409.
Duin, R. M., and van der Laan, H. (1972). *Astrophys. Lett.* **12**, 177.
Erickson, W. C., Kuiper, T. B. H., Clark, T. A., Knowles, S. H., and Broderick, J. J. (1972). *Astrophys. J.* **177**, 101.
Gower, J. F. R. (1967). *Nature* **213**, 1213.
Hewish, A., and Okoye, S. E. (1964). *Nature* **203**, 171.
Hogg, D. E., Macdonald, G. H., Conway, R. G., and Wade, C. W. (1969). *Astrophys. J.* **74**, 1206.
Kostenko, V. I., and Matveyenko, L. I. (1970). *Izv. Vyssh. Uchebn. Zaved. Radiophys.* **13**, 1467.
Lastochkin, V. P., Lukin, E. B., Stankevich, K. S., and Tzeitlir, N. M. (1965). *Sov. Astron.* **42**, 705.

Matveyenko, L. I. (1968). *Sov. Astron.* **45**, 160.
Matveyenko, L. I. (1969). *Sov. Astron.* **46**, 250.
Matveyenko, L. I. (1971). *Sov. Astron.* **48**, 1154.
Matveyenko, L. I. (1975). *Sov. Astron. Lett.* **7**, 13.
Matveyenko, L. I., and Artjuch, V. S. (1966). *Sov. Astron.* **43**, 2.
Matveyenko, L. I., and Conklin, E. K. (1972). *Sov. Astron.* **49**, 895.
Matveyenko, L. I., *et al.* (1973). *Sov. Astron.* **50**, 1157.
Matveyenko, L. I., and Lotova, N. A. (1970). *Sov. Astron.* **47**, 483.
Matveyenko, L. I., Martirosjan, R. M., and Sorochenko, R. L. (1965). *Sov. Astron.* **42**, 316.
Matveyenko, L. I., and Meeks, M. L. (1972). *Sov. Astron.* **49**, 965.
Matveyenko, L. I., and Pynzar, A. V. (1969). *Sov. Astron.* **46**, 550.
Mayer, C. H., and Hollinger, J. P. (1968). *Astrophys. J.* **151**, 53.
Montgomery, J. M., Epstein, E. E., Oliver, J. P., Dworetsky, M. M., and Fogarty, W. G. (1971). *Astrophys. J.* **167**, 77.
Seeger, C. L., and Westerhout, G. (1957). *Bull. Astron. Inst. Neth.* **13**, 312.
Slee, O. B. (1977). *Aust. J. Phys. Astrophys. Suppl.* No. 43.
Vandenberg, N. R., *et al.* (1973). *Astrophys. J.* **180**, L27.
Wilson, A. S. (1972). *Mon. Not. R. Astron. Soc.* **157**, 229.
Woltjer, L. (1957). *Bull. Astron. Inst. Neth.* **13**, 301.

Manuscript received 17 July 1978